

# Outdoor Sound Propagation Reference Model Developed in the European Harmonoise Project

Jérôme Defrance<sup>1</sup>, Erik Salomons<sup>2</sup>, Ingrid Noordhoek<sup>2</sup>, Dietrich Heimann<sup>3</sup>, Birger Plovsing<sup>4</sup>, Greg Watts<sup>5</sup>, Hans Jonasson<sup>6</sup>, Xuetao Zhang<sup>6</sup>, Eric Premat<sup>1</sup>, Isabelle Schmich<sup>1</sup>, François Aballea<sup>1</sup>, Marine Baulac<sup>1</sup>, Foort de Roo<sup>2</sup>

<sup>1</sup>: CSTB, 24 rue Joseph Fourier, F-38400 Saint-Martin-d'Hères, France. j.defrance@cstb.fr

<sup>2</sup>: TNO Science and Industry, P.O. Box 155, NL-2600 AD Delft, The Netherlands

<sup>3</sup>: DLR Institute of Atmospheric Physics, Oberpfaffenhofen, D-82234 Weßling, Germany

<sup>4</sup>: DELTA, Akademivej Building 356, DK-2800 Lyngby, Denmark

<sup>5</sup>: TRL, Old Wokingham Road, Crowthorne Berkshire, RG45 6AU, United Kingdom

<sup>6</sup>: SP, Box 857, SE-501-15 Borås, Sweden

## Summary

The *Harmonoise* reference model has been developed in order to predict long-term average sound levels in road and railway situations that are geometrically relatively simple but physically complex. The present paper describes all steps of calculations with this powerful model which includes several advanced numerical propagation methods to calculate the coupled effects of atmosphere, ground surface and obstacles on sound waves. The reference model employs a statistical description of the atmosphere, based on local meteorological data, as well as various impedance models for ground surfaces and other absorbing surfaces. Validations against *in situ* long-term measurements have been achieved in several sites; agreement between reference model and experimental results ranges from excellent in flat terrain situations down to fairly good in more complex configurations (hilly, viaduct).

PACS no. 43.28.Js, 43.28.Fp, 43.50.Vt

## 1. Introduction

Outdoor sound propagation under complex environment has been widely studied during the 30 past years [1, 2, 3] and the need for improving predicting methods is still a topical domain when computational costs are constantly decreasing. In this perspective new hybrid approaches have been proposed recently [4, 5]. The *Harmonoise* reference model is concerned with this problematics and consists of a collection of numerical codes which can be used to calculate accurate 'reference solutions' for situations that are geometrically relatively simple but physically complex. A typical example is a situation with non-linear wind speed profiles near a noise barrier. The 'reference solutions' may be used to assess the accuracy of the *Harmonoise* engineering model, but may also be used for other purposes, such as parameter studies of complex atmospheric effects on sound waves.

The reference model is suited for situations with a long road or railway with a noise barrier on one or both sides of the sound sources. Sound propagation around the vertical ends of the barriers (horizontal diffraction) is ignored. The

model employs various numerical propagation methods to calculate effects of the atmosphere, ground surface and obstacles on sound waves: the Parabolic Equation (PE), the Boundary Element Method (BEM) and the straight-ray model (RAY).

The present paper globally describes all elements of the reference model developed within the activity of Work Package 2 of the *Harmonoise* project [5, 6, 7, 8, 9, 10, 11], whereas the source description of trains and road vehicles was the aim of Work Packages 1.1 and 1.2 [12, 13]. The model is finally validated against long-term *in situ* measurements [14] and then used as a reference tool for the development and fine tuning of the engineering model of Work Package 3 [15].

## 2. Structure of the model

The objective of the reference model is the calculation of the long-term average sound levels  $L_{den}$  (day-evening-night) and  $L_{night}$  which are the two noise indicators that should be applied in the framework of in the European Directive 2002/49/EC relating to the assessment and management of environmental noise (25 June 2002). In section 2.1 formulas are given for a basic element of the calculation: the summation of sound levels from point sources

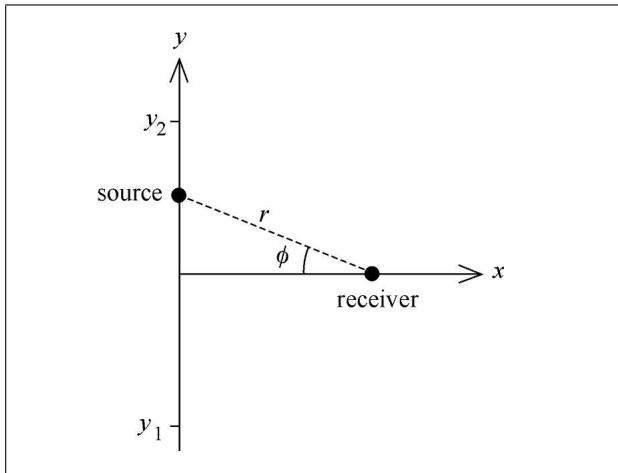


Figure 1. Geometry with a point source on the  $y$ -axis and a receiver at position  $(x, 0)$  on the  $x$ -axis.

moving along a line [6]. section 2.2 describes basic concepts of the reference model. section 2.3 specifies all steps of a calculation of long-term average sound levels with the reference model.

### 2.1. Basic formulas

In this section formulas are given for the equivalent sound level generated by incoherent point sources moving with constant speed along a line. The equi-angular distribution of incoherent point sources over the line is referred to as an *incoherent line source*.

The geometry is shown in Figure 1. A rectangular  $xy$  coordinate system in the horizontal plane is used. Point sources move along the  $y$ -axis, from  $y = y_1$  to  $y = y_2$ . The receiver is located at position  $(x, 0)$  on the  $x$ -axis. Angle  $\phi$  runs from  $\phi_1 = \arctan(y_1/x)$  to  $\phi_2 = \arctan(y_2/x)$ .

The average number of point sources per unit length is  $Q/v$ , where  $Q$  is the number of point sources passing per unit time and  $v$  is the speed of the point sources. The sound power level of a point source is written as

$$L_W(\phi) = L_{W,0} + \Delta L_W(\phi), \quad (1)$$

where  $L_{W,0}$  is a constant and  $\Delta L_W$  is a function of angle  $\phi$ , which represents horizontal directivity of the point source.

The *instantaneous* sound level generated by an individual point source passing from  $y_1$  to  $y_2$  varies in time. The *equivalent* sound level generated by the constant flow of point sources can be expressed as [6]:

$$L_{eq} = L_{W,0} + 10 \log(Q/v) - A_{line}, \quad (2)$$

where  $A_{line}$  is called line-source attenuation and ‘log’ stands for logarithm to the base 10. The sum  $L_{W,0} + 10 \log(Q/v)$  is called sound power level per unit length.

For numerical calculation of  $A_{line}$ , the line segment from  $y_1$  to  $y_2$  is divided into a number of smaller segments. As shown in Figure 2, segment  $j$  has length  $\delta y_j$ , and corresponds to angular interval  $\delta \phi_j$ . Segment  $j$  is represented

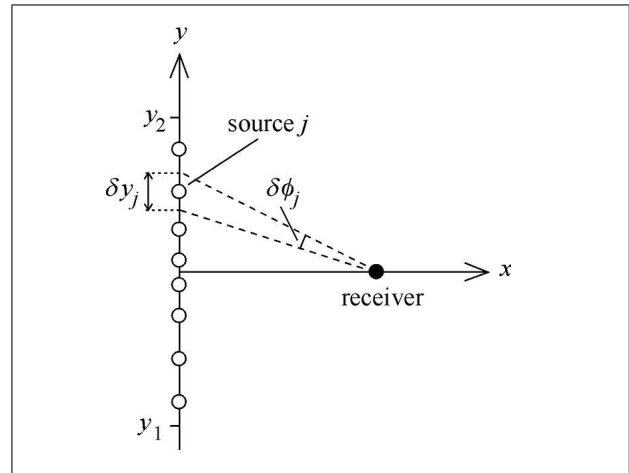


Figure 2. Point source  $j$  represents linear interval  $\delta y_j$  and angular interval  $\delta \phi_j$ .

by a (fixed) point source  $j$  at the center of the segment. Line-source attenuation  $A_{line}$  is then given by:

$$A_{line} = -10 \log \left( \sum_j 10^{[\Delta L_{W,j} - 10 \log(4\pi r_j^2) - A_{excess,j}]/10} \delta \phi_j \right), \quad (3)$$

where  $j$  runs over all segments between  $y = y_1$  and  $y = y_2$ , and  $x$  is the normal distance between the line source and the receiver (Figure 1). Quantity  $A_{excess,j}$  is the excess attenuation for propagation from point source  $j$  to the receiver, and represents effects of ground, meteorology, barriers and air absorption. One may note that this excess attenuation is defined as free field sound pressure level minus actual sound pressure level.

In exceptional cases, distance  $x$  is zero (for example, if the receiver is located on the  $y$  axis at  $y > y_2$ ) and the above expression for  $A_{line}$  fails. In these cases the following expression is used [16]:

$$A_{line} = -10 \log \left( \sum_j 10^{[\Delta L_{W,j} - 10 \log(4\pi r_j^2) - A_{excess,j}]/10} \delta y_j \right), \quad (4)$$

where  $r_j$  is the distance from point source  $j$  to the receiver. In the limit  $\delta y_j \rightarrow 0$  this expression is identical to equation (3).

To keep the number of numerical calculations as small as possible, it is important to use a distribution of point sources in Figure 2 for which the point sources have nearly equal contributions to the sound level at the receiver. In a free-field situation (homogeneous atmosphere, no air absorption, no ground, no obstacles), the contributions are equal for an *equi-angular* distribution, i.e. a distribution with a *constant* angular interval  $\delta \phi_j$ . The equi-angular distribution is also used for non-free-field situations. For the angular interval values of typically 5 to 20 degrees are used depending on the degree of accuracy required.

## 2.2. Basic concepts of the reference model

### 2.2.1. Main assumptions

It is assumed that vehicles move along straight lines representing roads (or railways). Curved roads (or railway

tracks) may be handled as a series of straight segments. There may be noise barriers on either side of the sound sources. The model takes into account reflection on the barriers and diffraction by their top edges. Situations with significant side effects of finite barrier are excluded by ignoring diffraction by their vertical edges

Each vehicle is represented by a number of incoherent point sources. Each point source moves along with the vehicle and leads to an incoherent line source. Consequently, a flow of vehicles on a road is modelled by a number of incoherent line sources at different heights and positions. For the calculation of sound levels, each incoherent line source is represented by a number of fixed point sources, as described in section 2.1.

### 2.2.2. Propagation planes

For each fixed point source, a number of *propagation planes* are considered (Figure 3) [10]. A propagation plane is a vertical plane that contains all sound rays from the source to the receiver with a fixed number of 'zigzag' reflections (and diffractions) between the two barriers shown in Figure 3. One neglects the fact that not all sound rays with a fixed number of zigzag reflections are exactly confined to a propagation plane, since diffracted rays follow Keller's law.

Propagation plane 1 contains all rays without reflections and diffractions by barrier 2 (Figure 3); Propagation plane 2 contains all rays reflected and diffracted by barrier 2. Propagation plane 3 contains all rays reflected and diffracted first by barrier 1 and next by barrier 2. And so on for the next propagation planes.

For a road without barriers, or a road *with* barrier 1 but *without* barrier 2, only propagation plane 1 is considered. For a road *with* barrier 2 but *without* barrier 1, propagation planes 1 and 2 are considered. For a road with both barrier 1 and barrier 2, the number of propagation planes taken into account depends on the propagation model (RAY, BEM, or PE) that is used in the source region.

If propagation model RAY or PE is used, calculation of separate contributions from propagation planes is straightforward. In this case, contributions from propagation planes 1, 2 and 3 are taken into account and contributions from propagation planes 4, 5, ... are neglected which is consistent with what has been observed in most cases [10, 17].

If propagation model BEM is used, however, contributions from different propagation planes cannot be separated by means of a single BEM calculation. Therefore, two BEM calculations are performed:

- i) a calculation for the situation *with* barrier 1 but *without* barrier 2,
- ii) a calculation for the situation *with* both barrier 1 and barrier 2.

Calculation i) yields the contribution from propagation plane 1. The difference of calculation ii) and calculation i) yields an approximation of the contribution from all other propagation planes. Thus, contributions from all propagation planes are taken into account in an approximate way.

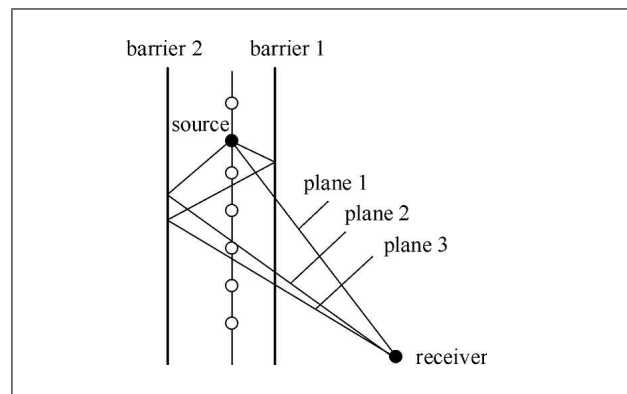


Figure 3. Top view of propagation planes 1, 2, and 3 for a point source in a situation with barriers on either side of the road. Each barrier reflection corresponds to a kink in a propagation plane.

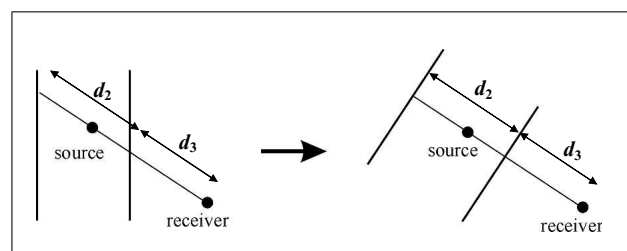


Figure 4. General illustration of the two-dimensional approximation. A situation with barriers at an arbitrary angle to the source receiver line (left) is replaced by a situation with barriers perpendicular to the source receiver line (right).

Coherence loss due to the turbulent state of the atmosphere [10] between propagation planes 2, 3, etc. cannot be accounted for in this case.

### 2.2.3. Two-dimensional approximation

For the calculation of excess attenuation, two-dimensional sound propagation models are used. Therefore, the *two-dimensional approximation* is used, for each propagation plane [8] except when the three-dimensional RAY model is used. This approximation is illustrated in Figure 4. Barriers are rotated such that they become perpendicular to the source-receiver line. After rotation, a two-dimensional propagation model is applied in the vertical plane through the source and the receiver to calculate excess attenuation. The two-dimensional approximation for propagation plane 2 is illustrated in Figure 5. The error introduced by this barrier rotation has been discussed in reference [10] and has been found to be less than 1 dB(A) in a complex case such as a train over a ballast-like boundary close to a noise barrier.

### 2.2.4. Source region

For the calculation of excess attenuation, a propagation plane is divided into two regions: a *source region* and the region outside the source region [10] (Figure 6). The source region extends to typically 2 m behind the barrier between the source and the receiver. If there is no barrier, the distinction between the two regions can be ignored.

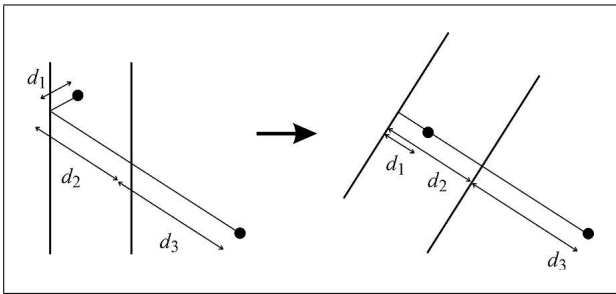


Figure 5. Illustration of the two-dimensional approximation for propagation plane 2. Distances  $d_1$ ,  $d_2$ , and  $d_3$  in the original geometry (left) are used in the approximate geometry (right).

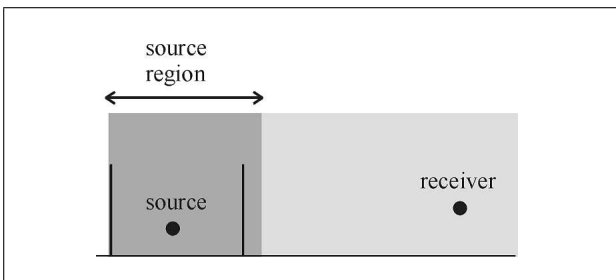


Figure 6. A propagation plane is divided into two regions: a source region (dark grey) and the region outside the source region (light grey).

Depending on the situation, different propagation models may be used in the source region and the region outside the source region (more detailed description in section 4).

### 2.3. Stepwise description of a reference model calculation

The stepwise description of the reference model is as follows:

**Step 1: Source description.** Sources are specified in terms of vehicle types, numbers of vehicles per hour (traffic flows), and vehicle speeds. Each vehicle is represented by a set of point sources at different heights. Consequently, a traffic flow is represented by a set of incoherent line sources. Each incoherent line source is represented by a set of (fixed) point sources.

**Step 2: Atmosphere.** A set of logarithmic-linear (called ‘loglin’) sound speed profiles is specified ( $m = 1, 2, \dots, M$ ) [18, 19]:

$$c_m(z) = c_0 + a_m \ln(1 + z/z_0) + b_m z, \quad (5)$$

where  $c_m$  is the (effective) sound speed as a function of height  $z$ ,  $c_0 = 340$  m/s is a constant sound speed, ‘ln’ stands for natural logarithm,  $z_0$  is the roughness length of the ground surface, and  $a_m$  and  $b_m$  are parameters that vary with index  $m$ . The number of profiles  $M$  is typically 25. Typical values of the parameters are  $z_0 = 0.1$  m,  $a_m = -1.0, -0.4, 0, 0.4, 1.0$  m/s and  $b_m = -0.12, -0.04, 0, 0.04, 0.12$  1/s (five values of  $a_m$  and five values of  $b_m$  yield 25 sound speed profiles). The 25 profiles include

both downward-refracting profiles and upward-refracting profiles. A more detailed description of equation (5) is given in section 4.4.1. Long-term average sound levels are calculated by weighted averaging of levels for the 25 profiles. The statistical weights of the profiles are denoted as  $w_m$ , with  $\sum_m w_m = 1$ . The statistical weights depend on local climate, propagation direction and period of the day. For a  $L_{den}$  assessment, each period (day, evening and night) has its own weights. Near obstacles such as noise barriers, range-dependent sound speed profiles are determined when necessary, as described in section 4.4.3.

**Step 3: Ground and absorbing surfaces.** Acoustic impedances of ground surfaces and other absorbing surfaces are specified. Various impedance models are available to calculate the impedance from a few empirical parameters, such as the air flow resistivity of the surface material. The topography of the ground surface is specified. It is assumed that the road surface is flat (apart from noise barriers). The ground surface outside the source region may contain gentle hills.

**Step 4: Propagation calculations.** Using a (possibly hybrid) propagation model, excess attenuations

$A_{\text{excess},m,j,i,p,n}$  are calculated for

- all sound speed profiles  $m = 1, 2, \dots, M$ ,
- all point sources  $j = 1, 2, \dots$ ,
- all incoherent line sources  $i = 1, 2, \dots$ ,
- all propagation planes  $p = 1, 2, 3$ ,
- all 1/3-octave bands  $n = 14, 15, \dots$  (with  $n$  defined below).

One-third octave band levels are derived from results for four frequencies per band:

$$f = f_c 10^{-3/80}, \quad f_c 10^{-1/80}, \\ f_c 10^{1/80}, \quad \text{and} \quad f_c 10^{3/80},$$

where  $f_c = 10^{n/10}$  is the mid-frequency of the band, with  $n = 14$  for 25 Hz,  $n = 15$  for 31.5 Hz, etc. Computer time and memory of the propagation models increase sharply with frequency, so it is often necessary to use an upper frequency band of 2.5 kHz, for example, and neglect contributions from higher bands. The choice of four frequencies per third-octave band is a result of preliminary simulations showing that this is a good compromise between calculation times and a global accuracy of 0.5 dB(A) compared to a narrow band result.

The propagation calculations are performed for a non-turbulent atmosphere. Effects of atmospheric turbulence are taken into account afterwards by setting an upper limit of 15 dB to the excess attenuation without including the attenuation due to air absorption. This value is coherent with measurements results presented in reference [20]. This approximate approach accounts for turbulent scattering of sound waves into a shadow region. More accurate values of the upper limit for specific situations may be determined by performing sound propagation calculations for a set of random simulations of the turbulent atmosphere, using appropriate values of turbulence parameters [10, 21, 22]. In

particular in a shadow region behind a high noise barrier, excess attenuation higher than 15 dB is possible.

The propagation calculations are performed for a non-dissipative atmosphere. Air absorption of sound energy of pure tones is taken into account afterwards by adding a term  $\alpha r$  to the excess attenuation, where  $r$  is the horizontal propagation distance and  $\alpha$  is the absorption coefficient (for 1/3 octave bands, see Sec. 4.4.5). The absorption coefficient is calculated with ISO 9613-1 [23], using appropriate average values of the temperature and the relative humidity.

**Step 5: Long-term average sound levels.** Long-term average sound levels are calculated by successive summation over sound speed profiles, point sources, incoherent line sources, and propagation planes.

First, excess attenuation is averaged over sound speed profiles by weighted summation with statistical weights  $w_m$  ( $m = 1, \dots, M$ ):

$$A_{\text{excess},i,j,p,n} = -10 \log \left( \sum_m w_m 10^{-A_{\text{excess},i,j,p,m,n}/10} \right). \quad (6)$$

From point-source excess attenuations  $A_{\text{excess},i,j,p,n}$ , line-source attenuation  $A_{\text{line},i,p,n}$  is calculated with equation (3), or, if necessary, with equation (4). Corresponding equivalent sound levels  $L_{\text{eq},i,p,n}$  are calculated with equation (2), taking into account the appropriate sound power levels, traffic flows, and speeds. Next, equivalent levels  $L_{\text{eq}}$  are calculated by summation over propagation planes, incoherent line sources, and 1/3-octave bands:

$$L_{\text{eq}} = 10 \log \left( \sum_n \sum_i \sum_p 10^{L_{\text{eq},i,p,n}/10} \right). \quad (7)$$

Finally, equivalent levels for the periods ‘day’, ‘evening’, and ‘night’, denoted as  $L_d$ ,  $L_e$ , and  $L_n$ , respectively, are combined into a day-evening-night level:

$$L_{\text{den}} = 10 \log \left( \frac{12}{24} 10^{L_d/10} + \frac{4}{24} 10^{(L_e+5)/10} + \frac{8}{24} 10^{(L_n+10)/10} \right). \quad (8)$$

The day period is 12 hours, the evening period is 4 hours and the night period is 8 hours. The start of the day (and consequently the start of the evening and the start of the night) can be chosen by each EU member State; the default values for the day, evening and night period are 07.00 to 19.00, 19.00 to 23.00 and 23.00 to 07.00, respectively. For the evening period there is a 5 dB ‘penalty’ and for the night period there is a 10 dB ‘penalty’.

Day level  $L_d$ , evening level  $L_e$ , and night level  $L_n$  differ because of:

- differences in sound emission, due to differences in traffic intensity and speed,
- differences in sound propagation, due to differences in meteorological conditions.

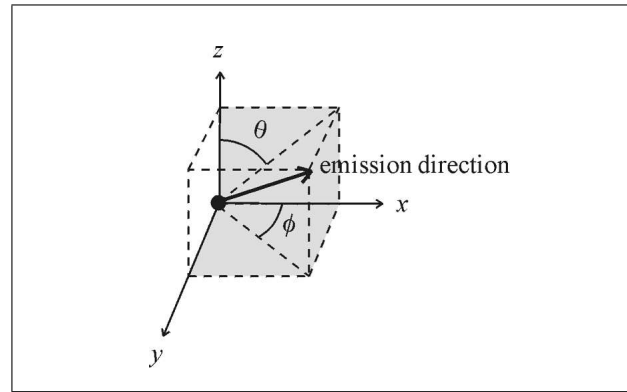


Figure 7. Angles  $\phi$  and  $\theta$  characterize the direction of sound emission of a point source on an incoherent line source directed along the (horizontal)  $y$ -axis.

The sound power spectra in equation (2) are A-weighted, so the resulting levels are also A-weighted.

Sound level contributions from different propagation planes are summed *incoherently*, while contributions from sound rays within a propagation plane are summed *coherently*. If necessary, one may use partial coherent summation depending on the turbulent state of the atmosphere [10], if the required turbulence parameters are known.

### 3. Sound emission

As described in section 2.2, each vehicle is represented by a number of incoherent point sources. In principle, the sound power spectrum  $L_W$  of each point source covers the frequency range from 25 Hz to 5 kHz. In practice, it may be necessary to neglect contributions from the highest frequency bands, due to limitations of the propagation models.

The sound power spectrum  $L_W$  of a point source may depend on emission direction (see section 2.1). Horizontal and vertical directivity are distinguished. Horizontal directivity corresponds to angle  $\phi$  and vertical directivity corresponds to angle  $\theta$  (Figure 7). Horizontal directivity is taken into account by using different sound power spectra for different angles of propagation. Vertical directivity should be taken into account in the propagation model. Most propagation models assume a monopole point source (and thus ignore directivity), but a directional source can in principle always be represented by a set of monopole sources with fixed phase relations [10].

## 4. Sound propagation

### 4.1. Description of the sound propagation models

This section presents brief descriptions of the main propagation models: several PE models, RAY and BEM. Other methods such as the Linearized Euler model (LE), the Meteo-Boundary Element Method (meteo-BEM), the Fast Field Program (FFP) and the curved-ray model with linearized sound speed profile (curved-RAY) have also been

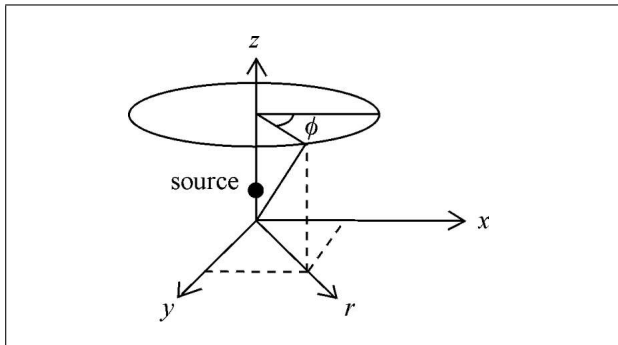


Figure 8. PE models assume that the sound field is independent of the azimuthal angle  $\phi$ , so calculations are performed in two dimensions in the vertical plane through the source and the receiver.

investigated; they are not presented here but more details may be found elsewhere [7, 10].

### CNPE

The Crank–Nicholson Parabolic Equation (CNPE) model yields a numerical solution of a PE for sound propagation [24, 25, 26]. The PE follows from the Helmholtz equation, i.e. the wave equation in the frequency domain, by considering one-way sound propagation from the source to the receiver (backscattering is neglected). The PE model is a two-dimensional model, based on the axisymmetric approximation illustrated in Figure 8. The calculation is performed on a rectangular grid in the vertical plane through the source and the receiver (Figure 9a). CNPE gives accurate results for sound waves travelling at elevation angles of up to about  $30^\circ$ .

The Helmholtz equation in the  $rz$  plane is

$$\frac{\partial^2 q}{\partial r^2} + \frac{\partial^2 q}{\partial z^2} + k^2 q = 0, \quad (9)$$

where  $q = p\sqrt{r}$ ,  $p = p(r, z)$  the (complex) sound pressure and  $k = \omega/c$  the wave number, with angular frequency  $\omega$  and (effective) sound speed  $c = c(r, z)$ . The corresponding PE is

$$\frac{\partial \psi}{\partial r} = Q\psi, \quad (10)$$

where variable  $p$  has been replaced by variable  $\psi = p\sqrt{r} \exp(-ik_0 r)$ , with constant wavenumber  $k_0$ , and  $Q$  is a differential operator that contains the second vertical derivative  $\partial^2/\partial z^2$ .

A calculation with the CNPE model is basically a finite-difference integration of the sound field in positive  $r$  direction, based on equation (10). The calculation starts at the source at  $r = 0$ , with a Gaussian starting field  $p(r = 0, z)$  that represents a (monopole) point source (except if RAY or BEM is used in the source region as pointed out in section 4.3). The grid spacing is of the order of one tenth of a wavelength, both in horizontal and in vertical direction. At the top of the grid an artificial sound-absorbing layer is used to eliminate spurious reflections.

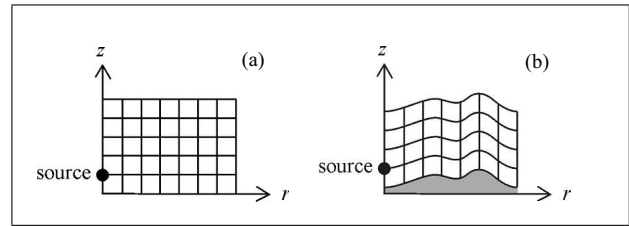


Figure 9. Rectangular grid in the  $rz$  plane (a); GTPE grid with terrain-following coordinates (b).

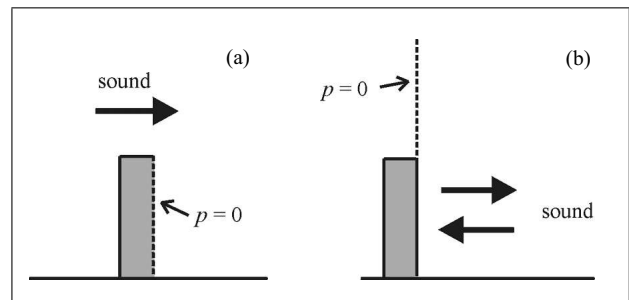


Figure 10. Illustration of the Kirchhoff approximation: (a) for propagation over a rectangular obstacle, (b) for reflection from a rectangular obstacle.

The effect of atmospheric refraction is taken into account by the effective sound speed approximation [26]. The effective sound speed is the sum of the adiabatic sound speed, which is a function of the temperature, and the horizontal wind speed component in the direction of sound propagation (see hereafter section 4.3). The effective sound speed is specified at each grid point, so height and range dependence of the effective sound speed is taken into account. At some places in this paper, the effective sound speed is referred to simply as the sound speed.

In situations with a flat ground surface without obstacles, the effective sound speed is a function of height only, and loglin profiles (2.5) are used. In situations with obstacles or hills, the effective sound speed varies with height and range, and a CFD (computational fluid dynamics) calculation of flow over an obstacle may be necessary (sound propagation over hills is calculated with GTPE).

At the ground surface, an impedance boundary condition is used. The ground impedance as a function of frequency is calculated from a few empirical parameters (presented hereafter in section 4.4), such as the air flow resistivity of the ground.

A rectangular obstacle on the ground surface can be taken into account with PE through the Kirchhoff approximation [27] whose accuracy has already been discussed elsewhere [17]. For *propagation over an obstacle* this means that the sound pressure at the back surface of the obstacle is set equal to zero (Figure 10a). For *reflection from an obstacle* this means that the sound pressure above the reflecting surface is set equal to zero upon reflection (Figure 10b). The sound-absorbing properties of the surface of the obstacle are ignored in the first case (Figure 10a), but may be taken into account approximately in

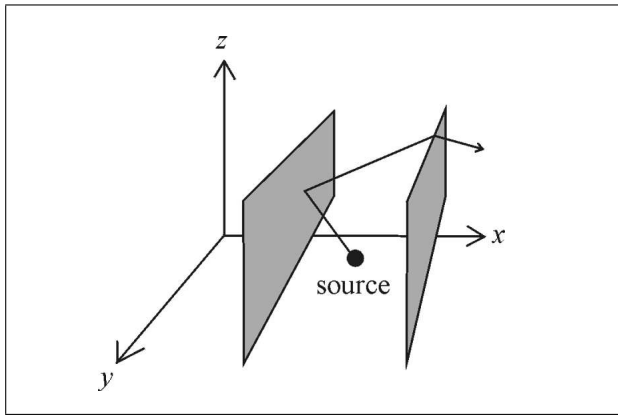


Figure 11. Example of a sound ray emitted by a source between two noise barriers. The ray has a reflection at the left barrier and a diffraction at the right barrier.

the second case (Figure 10b) by including a constant (real) reflection factor in the amplitude upon reflection.

**GFPE**

The Green’s function Parabolic Equation model [26, 28, 29] is in many ways similar to the CNPE model. A major difference is that with GFPE larger range steps are possible than with CNPE: the horizontal grid spacing with GFPE can be as large as 5 to 50 wavelengths, rather than one tenth of a wavelength with CNPE. Another advantage of GFPE is that accurate results can be obtained up to higher elevation angles than with CNPE, provided an appropriate higher-order starting field is used [26]. With a fourth-order starting field accurate results up to 60° are obtained. A presentation on how the GFPE is solved numerically can be found in references [29, 30].

**GTPE**

The Generalized Terrain Parabolic Equation (GTPE) model is a generalization of the CNPE model for sound propagation over a ground surface with smooth hills [26, 31]. Terrain-following coordinates are used (Figure 9b) rather than the rectangular grid shown in Figure 9a. GTPE gives accurate results for smooth hills with local slopes that do not exceed about 30°.

**RAY**

The ray model (RAY) used for the reference model is based on the theory of geometrical acoustics, and is described in reference [32]. Sound propagation from a (monopole) point source to a receiver is calculated by summation of contributions from sound rays. A ray consists of straight segments between reflection points and diffraction points. Reflection occurs at plane surfaces and diffraction occurs at wedges. An example is shown in Figure 11.

The (complex) sound pressure contribution of a sound ray is of the form:

$$p = QD \exp(ikR)/R, \tag{11}$$

where  $k$  is the wave number,  $R$  is the ray path length,  $Q$  is a product of spherical-wave reflection coefficients, and  $D$

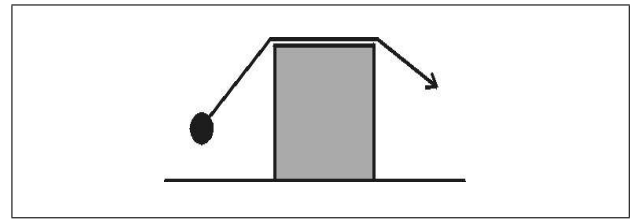


Figure 12. The ray model works for double diffraction at the top of a wide barrier if the top surface is rigid, but not if the top surface is absorbing.

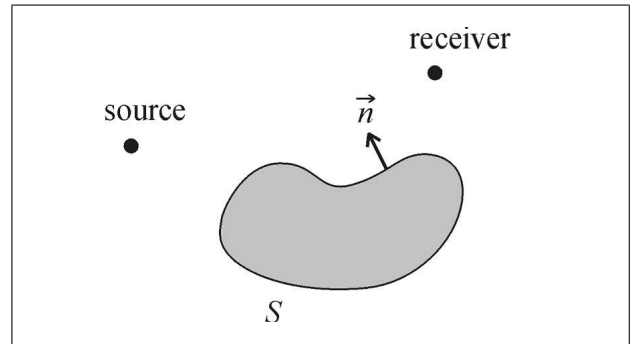


Figure 13. General geometry for BEM with a source, a receiver, and a scattering volume bounded by surface  $S$  and outward normal  $\vec{n}$ .

is a product of spherical-wave diffraction coefficients. The spherical-wave diffraction coefficient includes the option to model diffraction by an absorbing wedge, i.e. a wedge that consists of two finite-impedance surfaces. This approach works for diffraction by a single absorbing wedge, but gives inaccurate results for double diffraction by the top of a wide barrier (Figure 12). In the latter case, BEM (or PE) should be used rather than RAY. In cases with complex barrier shapes, BEM should be used.

In principle, the ray model is based on a high-frequency approximation. This means that all dimensions should be large compared to the wavelength. In many situations, however, the ray model works well down to frequencies where this condition is not fulfilled.

**BEM**

The BEM [7, 33, 34, 35] is based on the Kirchhoff-Helmholtz integral equation

$$C(\vec{r})p(\vec{r}) = 4\pi p_i(\vec{r}) - \iint_S \left[ G(\vec{r}, \vec{r}_0) \frac{\partial}{\partial n} p(\vec{r}_0) - p(\vec{r}_0) \frac{\partial}{\partial n} G(\vec{r}, \vec{r}_0) \right] d\vec{r}_0 \tag{12}$$

for complex sound pressure  $p(\vec{r})$  at receiver position  $\vec{r}$ , in the situation shown in Figure 13 with a monopole point source and an arbitrarily shaped scattering volume bounded by surface  $S$ . Green’s function  $G(\vec{r}, \vec{r}_0)$  is the free field at position  $\vec{r}_0$  due to a point source at position  $\vec{r}$ ,  $p_i(\vec{r})$  is the free field generated by the source, and  $\partial p/\partial n \equiv (\nabla p)\vec{n}$  is the derivative of  $p$  in the direction of normal vector  $\vec{n}$ . The second term on the right-hand side

represents the field due to the scattering volume.  $C$  is a geometrical coefficient that depends on position  $\vec{r}$ ;  $C$  is equal to  $2\pi$  if  $\vec{r}$  is on the surface  $S$  (not at a sharp corner) and equal to  $4\pi$  if  $\vec{r}$  is not on the surface. The reference model employs BEM in two dimensions (2D) since 2D and 3D calculations give very similar results in terms of excess attenuation [36]; therefore the surface integral in equation (12) becomes a line integral, and the Green's function is:

$$G(\vec{r}, \vec{r}_0) = i\pi H_0^{(1)}(k|\vec{r} - \vec{r}_0|), \quad (13)$$

where  $H_0^{(1)}$  is the Hankel function of the first kind and order zero. Equation (13) represents the field of a point source in 2D, corresponding to a coherent line source in 3D. For a point source above a finite-impedance ground surface, one may use a half-space Green's function, consisting of the direct term (4.1.5) plus an image term that accounts for the ground reflection [7].

Since equation (12) contains the unknown sound pressure  $p(\vec{r})$  on the left-hand side and the right-hand-side, two computational steps are required. First equation (12) is applied to positions  $\vec{r}$  on a fine grid that covers  $S$ , with a distance between neighbouring grid points of the order of one tenth of a wavelength. This yields a set of linear equations for the sound pressures at all grid points, which is solved numerically. In the second step these sound pressures are used in the right-hand-side of equation (12) to calculate the sound pressure at an arbitrary receiver position  $\vec{r}$ .

If  $S$  is a rigid surface, the normal derivative of the sound pressure vanishes on  $S$ , which implies that  $\partial p(\vec{r}_0)/\partial n$  in the integrand of the Kirchhoff-Helmholtz integral equation vanishes. If the impedance of  $S$  is finite, the following boundary condition is used:

$$\frac{\partial p}{\partial n} = -ik\beta p, \quad (14)$$

where  $\beta$  is the normalized admittance of the surface (normalized by the admittance of air).

A general problem with BEM is the so-called non-uniqueness problem [33]: at certain frequencies, corresponding to internal resonances of the scattering volume, inaccurate results are obtained. This problem is solved by including a number of points inside the scattering volume where the field is forced to be zero.

## 4.2. Benchmark calculations with sound propagation models

### 4.2.1. Definition of benchmark cases

An extensive benchmark calculations work has been carried out in order to select the different propagation methods suited for an efficient use in the reference model. Nine families of models have been tested and compared (when possible according to the limits of each of them): LE, BEM, Meteo-BEM, CNPE, GFPE, GTPE, FFP, RAY and curved-RAY.

A set of cases have been tested using typical values for propagation distances (20, 200 and 2000 m), source height (0.05, 0.5 and 5 m), receiver height (1.5 and 4 m), ground

or material characteristics (rigid, grassland, porous asphalt and porous concrete), meteorological profiles (8 types), impedance discontinuity geometry (4 cases), barrier geometry (8 cases) and terrain configuration (4 cases). A total of 313 cases has been thus investigated on a wide range of frequencies (24 bands, with mid-frequencies between 25 Hz and 5 kHz)

### 4.2.2. Analysis and conclusions

In many benchmark cases, two or more basic models agree, giving a reasonable reference for the 'exact' solution. We give here an overall indication of the performance of the models in the benchmark calculations. Three properties are evaluated: accuracy, applicability, and computational effort. Accuracy is based on deviation from the 'exact' solution. Applicability refers to limitations of the set of situations the model can be applied to. Computational effort refers to computing times and memory.

Concerning the **LE model**, the results are accurate in most cases, although there are some deviations near interference minima for impedance ground. With very recent improvements to LE model, the computational cost is not a limiting factor anymore and in principle this approach has no limitations in applicability. But at the time of the simulations and the choices of algorithms (2002), the integration of an impedance ground in the LE model showed very significant additional computing time and memory.

For the **BEM**, the results are also accurate in most cases. Attention has to be paid to the mesh size. The model is limited to a non-refracting atmosphere but can handle complex geometrical configurations. The computational effort is large (only 2D model investigated here).

The results of **Meteo-BEM** are accurate in many cases, but deviate from the 'exact' solution in some cases. The model is presently limited to linear profiles. The computational effort is large.

**CNPE and GFPE methods** show accurate results in many configurations. In some cases of upward refraction, CNPE results are inaccurate at high frequency. The models are limited to axisymmetric cases with a flat ground and maximum propagation angles between typically 35 and 70 degrees. Rectangular obstacles can be taken into account through the Kirchhoff approximation. The computational effort is large.

The **GTPE** results agree with results of GFPE with the conformal mapping approach [26]. Therefore the results are considered accurate. The model can handle arbitrary terrain profiles with maximum elevation angles of about 30 degrees. The model has the same limitations as the CNPE model with respect to axial symmetry and propagation angles. The computational effort is large.

For the **FFP**, the results are accurate in many cases, although there are some deviations from the 'exact' solution, in particular at high frequency. The model is limited to axisymmetric situations with a layered atmosphere and a flat homogeneous ground. The computational effort is large.

The **RAY** model is accurate in many cases, such as cases with a screen on a ground surface. The model is limited to

a non-refracting atmosphere and obstacles with flat surfaces. Dimensions of obstacles and distances to diffraction edges should be larger than the wavelength. The computational effort is small.

Concerning the **curved-ray model**, the results agree with the ‘exact’ solution in some cases, but show large deviations in other cases. Applicability of the model is the same as for RAY, except for the non-refracting atmosphere. The computational effort is small.

Hybrid models as **RAY + CNPE** and **BEM + CNPE** agree with other models in cases investigated. However a disadvantage of the hybrid models is that refraction in the source region is neglected.

### 4.3. Selection of propagation models

From the previous conclusions, three types of propagation methods are finally used in the reference model [7]:

- the Parabolic Equation methods: CNPE, GFPE, and GTPE,
- the straight-ray method,
- the Boundary Element Method.

One may note that the LE model is excluded from further consideration mainly because of its high computational demand.

In the source region, PE, RAY, or BEM is used. However, atmospheric refraction is taken into account by PE but not by RAY and BEM. Therefore, PE is applied in the source region if possible [10]. In the region outside the source region, PE is used. PE cannot be used for complex situations (for example, situations with tilted barriers or barriers with a complex shape) and for situations with sound waves propagating at large elevation angles. PE can handle screening and reflection by simple rectangular noise barriers through the Kirchhoff approximation. The discontinuous change of effective sound speed upon reflection may be taken into account.

If PE cannot be applied and if refraction may be neglected, RAY or BEM is used. BEM can handle arbitrary complex geometries, but is restricted to two-dimensional modelling due to computational limitations. RAY is a three-dimensional model (so the two-dimensional approximation mentioned in section 2 is not applied) but is restricted to relatively simple geometries.

The choice between PE and RAY or BEM corresponds to a choice between accurate modelling of atmospheric refraction and accurate modelling of a complex geometry. Both options imply an approximation: either the atmosphere in the source region is approximated by a non-refracting atmosphere, or the complex geometry is approximated by a simpler geometry. Which option is best depends on the situation.

In the region outside the source region, a PE model is used. For a flat ground surface, the CNPE model or the GFPE model is applied. For a ground surface with smooth hills, the generalized-terrain PE model (GTPE) is used. If RAY or BEM is chosen in the source region, the model is coupled to a PE model at the boundary of the source region (Figure 14). RAY or BEM produces a set of complex sound pressures that is used as a starting field for PE.

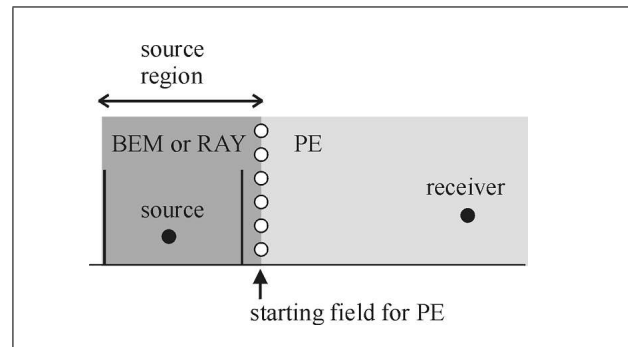


Figure 14. BEM or RAY is coupled to PE by generating a starting field for PE, consisting of a set of complex pressures at the boundary of the source region.

### 4.4. Atmosphere

This section describes how the set of effective sound speed profiles  $c_m(z)$ , given by equation (5), and corresponding statistical weights  $w_m$  ( $m = 1, 2, \dots, M$ ), are derived from local meteorological data.

#### 4.4.1. Effective sound speed profiles

The effective sound speed  $c$  is defined as the sum of the adiabatic sound speed  $c_{ad}$  and the wind speed component in the direction of sound propagation  $u$  [37]. The vertical profiles of  $c$ ,  $c_{ad}$ , and  $u$  are approximated by loglin functions:

$$c(z) \equiv c_{ad}(z) + u(z) \approx c_0 + a \ln(1 + z/z_0) + bz, \quad (15)$$

$$c_{ad}(z) = \sqrt{\kappa RT(z)} \approx c_0 + \frac{1}{2} \frac{\kappa R}{c_0} (T(z) - T_0) \\ \approx c_0 + a_c \ln(1 + z/z_0) + b_c z, \quad (16)$$

$$u(z) = V(z) \cos(\alpha(z) - 180^\circ) \\ \approx a_u \ln(1 + z/z_0) + b_u z, \quad (17)$$

$$\text{with } a = a_c + a_u, \quad b = b_c + b_u. \quad (18)$$

Here,  $z_0$  is the roughness length of the ground surface,  $\kappa = c_p/c_v = 1.4$  is the ratio of the specific heat capacities at constant pressure and constant volume, and  $R = 287 \text{ J/kg/K}$  is the specific gas constant of dry air. Further  $T_0$  and  $c_0 = \sqrt{\kappa RT_0}$  are the temperature and the sound speed at ground level, respectively,  $V(z)$  is the horizontal wind speed, and  $\alpha(z)$  is the angle between the wind direction and the direction of sound propagation. The wind direction is defined as the direction *from which* the wind is blowing ( $0^\circ$  for North wind,  $90^\circ$  for East wind, etc.) and the direction of sound propagation is defined as the direction *into which* sound waves travel ( $0^\circ$  for sound waves travelling to the North,  $90^\circ$  for sound waves travelling to the East, etc.).

If vertical profiles of wind speed, wind direction, and temperature are measured (with a meteorological mast or with a radio-acoustic sounding system, for example), the vertical profiles of the effective sound speed can be calculated directly, and the profile coefficients  $a$  and  $b$  in equation (15) can be determined with an appropriate curve fitting algorithm.

Table I. Wind speed classes W1 to W5 and according wind speeds  $V$  at 10 m above ground.

wind speed class	$V(z = 10\text{ m})$
W1	0 ... 1 m/s
W2	1 ... 3 m/s
W3	3 ... 6 m/s
W4	6 ... 10 m/s
W5	>10 m/s

Table II. Upwind/downwind classes V1 to V9 and according wind components  $u$  at 10 m above ground in the direction of sound propagation.

wind class	$u(z = 10\text{ m})$	
V1	< -10 m/s -10 ... - 6 m/s -6 ... - 3 m/s -3 ... - 1 m/s	upwind
V2		
V3		
V4		
V5	-1 ... + 1 m/s	crosswind
V6		downwind
V7		
V8		
V9	> +10 m/s	

Table III. Stability classes S1 to S5.

stability class	day/night, cloud cover (octas)
S1	day, 0/8 ... 2/8
S2	day, 3/8 ... 5/8
S3	day, 6/8 ... 8/8
S4	night, 5/8 ... 8/8
S5	night, 0/8 ... 4/8

In most cases, however, vertical profiles are not directly measured, and data are available only for a certain height above the ground. In these cases it is necessary to generate the profiles by assuming the validity of the surface-layer similarity theory, which relates the vertical turbulent fluxes of momentum and heat to three surface-layer scaling parameters: friction velocity  $u_*$ , Monin-Obukhov length  $L$ , and temperature scale  $T_*$ . The scaling parameters are used in empirical flux-profile relations.

If the vertical turbulent fluxes of momentum and heat are measured directly (with 3D ultrasonic probes, for example), the scaling parameters  $u_*$ ,  $L$  and  $T_*$  can be derived directly. If only routine meteorological data (weather station data) are available,  $u_*$ ,  $L$ ,  $T_*$  and the surface temperature  $T_0$  can be derived from Tables IV–VII, with meteorological propagation classes defined by Tables I–III. The classes depend on the following parameters:

- wind speed at 10 m above the ground,  $V(z = 10\text{ m})$ ,
- wind speed component in the direction of sound propagation at 10 m above the ground,  $u(z = 10\text{ m})$ ,

Table IV. ‘Projected’ friction velocity  $u_* \cos(\alpha - 180)$  in m/s for each upwind/downwind class.

wind class	$u_* \cos(\alpha - 180)$
V1	-0.87
V2	-0.53
V3	-0.30
V4	-0.13
V5	$\pm 0.00$
V6	+0.13
V7	+0.30
V8	+0.53
V9	+0.87

Table V. Inverse Monin-Obukhov length  $1/L$  in 1/m for wind speed classes W1 to W5 and stability classes S1 to S5.

	S1	S2	S3	S4	S5
W1	-0.08	-0.05	0	+0.04	+0.06
W2	-0.05	-0.02	0	+0.02	+0.04
W3	-0.02	-0.01	0	+0.01	+0.02
W4	-0.01	0	0	0	+0.01
W5	0	0	0	0	0

Table VI. Temperature scale  $T_*$  in K for classes W1 to W5 and stability classes S1 to S5.

	S1	S2	S3	S4	S5
W1	-0.4	-0.2	0	+0.2	0.3
W2	-0.2	-0.1	0	+0.1	0.2
W3	-0.1	-0.05	0	+0.05	0.1
W4	-0.05	0	0	0	0.05
W5	0	0	0	0	0

Table VII. Surface temperature  $T_0$  in °C for stability classes S1 to S5.

S1	S2	S3	S4	S5
+15	+15	+15	+5	+5

- cloud cover in octas,
- time of the day (day/night).

Once the surface-layer scaling parameters  $u_*$ ,  $L$  and  $T_*$  have been determined, the profile parameters  $a_u$ ,  $b_u$  in equation (16) and  $a_c$ ,  $b_c$  in equation (17) can be calculated with the help of flux-profile relations. The Businger-Paulson profiles (integrated Businger-Dyer flux-profile relations) are assumed [38, 39], but for the unstable case (day) the non-logarithmic term is replaced by a linear term [18]. The linearization is valid for  $z/L \geq -0.5$ , or  $z < 0.5|L|$  for  $L < 0$ . This approach results in the following expressions.

The wind component in the direction of sound propagation is given by

$$\begin{aligned}
 u(z) &= a_u \ln(1 + z/z_0) + b_u z, & (19) \\
 a_u &= \frac{u_* \cos(\alpha - 180^\circ)}{K}, \\
 b_u &= \frac{u_* \cos(\alpha - 180^\circ)}{K} \frac{1.0}{L} & \text{during day,} \\
 b_u &= \frac{u_* \cos(\alpha - 180^\circ)}{K} \frac{4.7}{L} & \text{during night.}
 \end{aligned}$$

The adiabatic sound speed is given by:

$$\begin{aligned}
 c_{ad}(z) &= c_0 + a_c \ln(1 + z/z_0) + b_c z, & (20) \\
 a_c &\approx \frac{1}{2} \frac{\kappa R}{c_0} 0.74 \frac{T_*}{K}, \\
 b_c &\approx \frac{1}{2} \frac{\kappa R}{c_0} \left( \frac{T_*}{K} \frac{0.74}{L} + \gamma_d \right) & \text{during day,} \\
 b_c &\approx \frac{1}{2} \frac{\kappa R}{c_0} \left( \frac{T_*}{K} \frac{4.7}{L} + \gamma_d \right) & \text{during night,}
 \end{aligned}$$

with the von Karman constant  $K = 0.4$ , the dry adiabatic vertical temperature gradient  $\gamma_d = -0.0097$  K/m.

Finally, profiles given in equations (19) and (20) are combined according to equation (18) to determine profile parameters  $a$  and  $b$  of the effective sound speed.

#### 4.4.2. Statistical weights

Each pair of profile parameters  $a$  and  $b$  describes a specific situation of sound propagation. To minimize the number of sound propagation calculations, the profile parameters are aggregated into a reasonable number of classes, labelled by index  $m$  in section 2.3. Each class is defined by intervals of  $a$  and  $b$ , and is represented by a specific pair of parameters out of the intervals. Propagation calculations are performed for the representative pairs of  $a$  and  $b$ . Statistical weights  $w_m$  in section 2.3 are equal to the frequencies of occurrence of the classes, determined on the basis of data collected for a period of at least one year.

In references [10, 19] the effect of the number of classes on calculated long-term average sound levels was investigated. It turned out that a number of 25 classes (five intervals of  $a$  times five intervals of  $b$ ) ensures a determination of long-term average sound levels with an error of at most 2 dB at 1000 m range. An example of a classification with 25 profiles is given in Tables VIII and IX.

#### 4.4.3. Range-dependent profiles near obstacles

An obstacle such as a noise barrier has an effect on sound waves but also on wind. Consequently, the loglin sound speed profiles described in the previous section are ‘disturbed’ in the neighbourhood of an obstacle. In general, one may use CFD calculations to determine the wind field around an obstacle. In references [26, 40] analytical formulas are given for the range-dependent profile near a noise screen, for a logarithmic inflow profile. The formulas are based on CFD calculations and wind tunnel measurements.

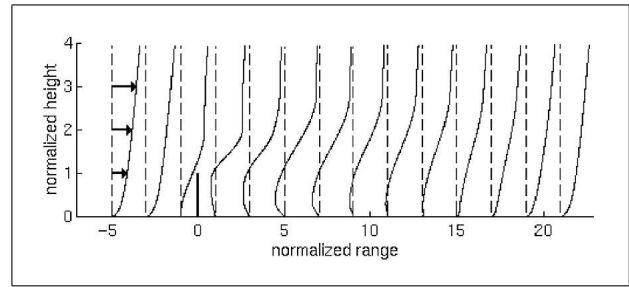


Figure 15. Range-dependent wind speed profiles near a 4 m high noise screen, for a loglin inflow profile  $u(z) = \ln(1 + z/z_0) + 0.2z$  perpendicular to the screen. Dimensions are normalized by the screen height.

In reference [10] these formulas are generalized to the case of a loglin inflow profile.

Figure 15 shows a typical example of disturbed wind speed profiles near a 4 m high noise screen, calculated with the formulas from reference [10] for a loglin inflow profile  $u(z) = \ln(1 + z/z_0) + 0.2z$  perpendicular to the screen. Dimensions in the figure are normalized by the screen height. Profiles are disturbed in the region between three screen heights upwind of the screen to twenty screen heights downwind of the screen. Outside this region the profiles are undisturbed.

#### 4.4.4. Turbulence

Atmospheric turbulence has two distinct effects on sound propagation

1. sound waves are scattered by turbulent eddies into shadow regions,
2. phase fluctuations due to turbulent eddies cause a loss of coherence of sound waves traveling along different paths, in particular along different propagation planes.

The first effect is taken into account in an approximate way, since sound levels in shadow regions are generally low, and low levels have a minor effect on long-term average levels. An upper limit of 15 dB is applied to the excess attenuation (not including attenuation due to air absorption; see section 2.3). More accurate values of the upper limit for specific situations may be determined by performing sound propagation calculations for a set of random realizations of the turbulent atmosphere, using appropriate values of turbulence parameters [10, 21, 22].

The second effect is also taken into account in an approximate way: contributions from different propagation planes are summed *incoherently* (section 2.3). If necessary, one may use partial coherent summation to account for the effect of atmospheric turbulence, if the required turbulence parameters are known.

#### 4.4.5. Air absorption

The effect of air absorption on sound propagation is calculated with ISO 9613-1 [23]. For a pure tone, the effect is a reduction of a received sound pressure level by  $\alpha r$ , where  $r$  is the horizontal propagation distance and  $\alpha$  is the absorption coefficient at the frequency of the tone. For broadband

Table VIII. Example of class intervals I and representative values V of the logarithmic profile parameter  $a$  in m/s.

I	$-\infty < a_1 \leq -0.7$	$-0.7 < a_2 \leq -0.2$	$-0.2 < a_3 \leq 0.2$	$0.2 < a_4 \leq 0.7$	$0.7 < a_5 \leq \infty$
V	$a_1 = -1.0$	$a_2 = -0.4$	$a_3 = 0$	$a_4 = 0.4$	$a_5 = 1.0$

Table IX. Example of class intervals and representative values of the linear profile parameter  $b$  in 1/m.

I	$-\infty < b_1 \leq -0.08$	$-0.08 < b_2 \leq -0.02$	$-0.02 < b_3 \leq 0.02$	$0.02 < b_4 \leq 0.08$	$0.08 < b_5 \leq \infty$
V	$b_1 = -0.12$	$b_2 = -0.04$	$b_3 = 0$	$b_4 = 0.04$	$b_5 = 0.12$

noise 1/3-octave bands are used, and the effect of air absorption is a reduction of a 1/3-octave band level by

$$A_{\text{air}} = \alpha r (1.0053255 - 0.00122622\alpha r)^{1.6}, \quad (21)$$

where  $\alpha$  is evaluated at the mid-frequency of each 3rd octave band [10].

The absorption coefficient  $\alpha$  according to ISO 9613-1 standard is a function of temperature and relative humidity. Average local values of these parameters are used. Values for the periods day, evening, and night are distinguished if possible.

#### 4.5. Ground and obstacles

Absorbing ground surfaces and other surfaces are represented by the normalized acoustic impedance  $Z$  (normalized by the impedance of air). Various empirical and theoretical models exist to calculate  $Z$  as a function of frequency from parameters that characterize the absorbing material, such as flow resistivity and porosity. The reference model employs four impedance models which are described in the Appendix.

In some cases a surface is modelled as a layer of porous material with a rigid backing. In these cases the impedance  $Z_{\text{layer}}$  is calculated from the normalized characteristic impedance  $Z$  of the porous material with the relation

$$Z_{\text{layer}} = Z \coth(-ikd), \quad (22)$$

where  $k$  is the complex wave number and  $d$  is the thickness of the porous layer.

Table X lists impedance models and parameters for various ground surfaces and absorbing surfaces. The values of the parameters in the table are ‘default values’, which may be replaced by more accurate values for specific cases (obtained from measurements). The description of the different impedance models used is given in the Appendix (Delany and Bazley, Hamet et al., exponential porosity and hybrid model).

In specific cases it may be necessary to include the effect of surface roughness as an effective contribution to the impedance of a surface. Various models exist to calculate this contribution [10].

#### 4.6. Barriers and hills

As described in section 4.1, the propagation methods PE, BEM, and RAY offer various possibilities to take into account the effects of obstacles and hills. BEM and RAY can be used for obstacles with a complex shape, but since refraction is ignored, these models are used only in the source region. CNPE and GFPE can be used for rectangular obstacles, but in this case there are limitations with respect to the elevation angle and the absorbing properties of the obstacles. GTPE can be used for propagation over smooth hills, with local slopes not exceeding about 30°.

A case of practical interest is a (rail) road on an embankment. If the embankment is not too wide, the sloping sides of the embankment may be included in the source region, and modelled by BEM or RAY. Otherwise, PE must be used. With CNPE or GFPE the sloping sides are approximated by a vertical step in the ground surface. If the embankment can be approximated as a smooth hill, GTPE can be used.

#### 4.7. Barrier tops

A ‘barrier top’, also called ‘crowning’, is a device installed at the top of a barrier aiming at improving the performance of the barrier without increasing its overall height. In principle, a barrier with a crowning can be considered as a complex shaped obstacle. The most common tops are the T and the cylinder [34, 35].

Sound propagation over a barrier with a ‘barrier top’ can be modelled by using BEM in the source region. Alternately, one may use PE in the source region and account for the effect of the barrier top by an analytical correction applied to the PE results. The analytical correction is developed on the basis of numerical BEM results [41] with a heuristic approach to account for refraction [11]. The alternate approach with PE should be used if the effect of refraction in the source region is expected to be larger than the effect of the barrier top.

### 5. Validations

#### 5.1. Validation of the reference model against *in situ* measurements

The outdoor sound propagation reference model has been validated by comparison with *in situ* long-term measurements results [14]. Local meteorological data recorded in

Table X. Impedance models and parameters for various ground surfaces and absorbing surfaces.

Surface/Ground type	Impedance model	Default parameters
concrete, (dense) asphalt, ice, water	rigid surface	$Z = \infty$
porous asphalt	Hamet et al.	$\sigma = 5 \text{ kPa s/m}^2, \Omega = 0.2, q^2 = 5, d = 0.04 \text{ m}$
compacted soil	Delany and Bazley	$\sigma = 2000 \text{ kPa s/m}^2, d = \infty$
grassland, cultivation land	Delany and Bazley	$\sigma = 200 \text{ kPa s/m}^2, d = \infty$
forest humus	exponential porosity	$\sigma = 8 \text{ kPa s/m}^2, \alpha = 25/\text{m}$
snow	Delany and Bazley	fresh/old snow: $\sigma = 5/30 \text{ kPa s/m}^2$ , thin/medium/thick layer: $d = 0.1/0.3/1.0 \text{ m}$
mixed ground (asphalt/grassland)	Delany and Bazley	100/67/ 50/ 33/ 0% of grass: $\sigma = 200/400/600/1000/\infty \text{ kPa s/m}^2$ with $d = \infty$
railway ballast bed (well defined)	Hamet et al.	$\sigma = 3 \text{ kPa s/m}^2, \Omega = 0.3, q^2 = 3, d = 0.4 \text{ m}$
railway ballast bed (unknown composition)	Delany and Bazley	$\sigma = 50 \text{ kPa s/m}^2, d = \infty$
porous concrete	Hamet et al.	$\sigma = 10 \text{ kPa s/m}^2, \Omega = 0.25, q^2 = 4, d = 0.1 \text{ m}$
mineral wool	hybrid	$\sigma = 50 \text{ kPa s/m}^2, \Omega = 0.9, q^2 = 2.5, d = 0.1 \text{ m}$

Table XI. Global results of validations against measurements for two typical studied sites. M: Microphone number,  $d_{\min}$ : Shortest distance to source [m],  $h_M$ : Microphone height [m],  $L_{\text{den}M}$ : Measured  $L_{\text{den}}$  [dB(A)],  $L_{\text{den}C}$ : Calculated  $L_{\text{den}}$  [dB(A)], Diff: Difference [dB(A)].

M	$d_{\min}$	$h_M$	$L_{\text{den}M}$	$L_{\text{den}C}$	Diff
Ladenburg II (highway, flat surroundings). Measurements duration: 32 days					
1	37	6	77.5	77.7	0.2
2	164	4	68.1	68.2	0.1
3	316	4	64.9	64.6	-0.3
4	558	4	60.2	60.6	0.4
5	1115	4	54.4	54.9	0.5
Unna (highway on embankment with barriers on both sides). Measurements duration: 19 days					
1	25	4	64.6	63.7	-0.9
2	150	4	62.5	61.8	-0.7
3	300	4	60.3	58.9	-1.4
4	550	4	57.8	56.2	-1.6

parallel with noise levels and traffic characteristics have been used together with physical data as input data. The validation of the reference model included nine measurement campaigns at six locations with a large variety of propagation and terrain conditions. Long-term  $L_{\text{den}}$  results are presented in Table XI for a couple of sites for which theoretical sound predictions have been achieved using the Parabolic Equation approach. From the comparisons with the measured results it appears that the agreement between reference model and experimental results ranges from fairly good in hilly terrain with the road on a viaduct (Maximum absolute differences between the calculated and the measured  $L_{\text{den}}$  of 3.1 dB(A)) up to excellent in flat terrain situations (Maximum absolute  $L_{\text{den}}$

differences less than 0.5 dB(A)). This conclusion encompasses road traffic noise, railway noise and point sources from a loudspeaker (Maximum absolute  $L_{\text{den}}$  differences of 2.3 dB(A) for the latter case).

The ambition levels of accuracy defined at the start of the *Harmonoise* project were: a 95%-confidence interval of the predicted values of  $\pm 1$  dB(A) for distances up to 100 m, a 95%-confidence interval of the predicted values of  $\pm 2$  dB(A) for distances up to 2000 m in flat terrain, and a 95%-confidence interval of the predicted values of  $\pm 5$  dB(A) for distances up to 2000 m in hilly terrain. For the reference model, the boundaries of the 95%-confidence interval are exceeded in only 2 out of the 49 cases examined. This means that in only 4% of the cases the difference is outside the 95%-confidence interval. In other words, the ambition for the reference model has been fulfilled.

## 5.2. Reference tool for the development of the *Harmonoise* engineering model

The reference model has been extensively used for the development and the validation of the engineering model [15]. An important set of cases have been tested using typical values for propagation distances (25 to 500 m), ground air flow resistivity (80 to 2000 kPa s/m<sup>2</sup>), barrier and embankment heights (0.5 to 4 m), and meteorological loglin profiles (logarithmic profile parameter  $a = -0.6$  to  $+0.6$  m/s, and linear profile parameter  $b = -0.12$  to  $+0.12$ /m). Computations have been carried out on a wide range of frequencies for more than 14700 different cases.

One essential aim of these tests was to check the sensitivity and the continuity of the engineering model with respect to input data. Attention has been paid to small variations of the terrain profile as well as low obstacle problems and transition between single and double diffraction.

## 6. Conclusions

An advanced numerical model has been developed within the framework of the European *Harmonoise* project. This so-called reference model is a collection of three families of sound propagation methods which may be coupled together: the PE model, the straight-ray approach and the BEM. This set of numerical codes allows to handle realistic road and railway configurations with range dependent sound speed profiles, and is able to deliver ultimately a 'reference'  $L_{\text{den}}$  value.

Work is still in progress in the frame of the European *Imagine* project in order to apply this reference model to aircraft noise as well as industrial noise. The reference model is also currently used to study complex outdoor sound problems such as the effect of meteorology on road traffic noise propagation in mountainous sites.

## Appendix: Impedance models

### Delany and Bazley model

Delany and Bazley [42] have developed an empirical model for fibrous absorbent materials, which is also used for natural grounds such as grassland. The expressions for  $Z$  and  $k$  are

$$Z = 1 + 0.0511\left(\frac{\sigma}{f}\right)^{0.75} + i0.0768\left(\frac{\sigma}{f}\right)^{0.73}, \quad (\text{A1})$$

$$\frac{k}{\omega/c} = 1 + 0.0858\left(\frac{\sigma}{f}\right)^{0.70} + i0.175\left(\frac{\sigma}{f}\right)^{0.59}. \quad (\text{A2})$$

The material is characterized by a single parameter: the air flow resistivity  $\sigma$ . Other independent parameters are: adiabatic sound speed  $c$  (in air), angular frequency  $\omega$ , and frequency  $f$ . One may note that the positive sign of the imaginary parts in the above equations corresponds to the choice of the harmonic time factor in sound propagation models.

### Hamet *et al.* model

Hamet *et al.* [43] have developed a theoretical model for porous media with a rigid frame. The expressions for  $Z$  and  $k$  are:

$$Z = \frac{q}{\Omega} F_{\mu}^{1/2} \left[ \kappa - \frac{\kappa-1}{F_{\theta}} \right]^{-1/2}, \quad (\text{A3})$$

$$\frac{k}{\omega/c} = q F_{\mu}^{1/2} \left[ \kappa - \frac{\kappa-1}{F_{\theta}} \right]^{1/2}, \quad (\text{A4})$$

with  $F_{\mu} = 1 + i f_{\mu}/f$ ,  $F_{\theta} = 1 + i f_{\theta}/f$ ,  $f_{\mu} = \Omega \sigma / (2\pi \rho q^2)$  and  $f_{\theta} = \sigma / (2\pi \rho N_{\text{Pr}})$ . Material parameters are: structure constant  $q^2$ , porosity  $\Omega$ , and air flow resistivity  $\sigma$ . Other quantities are: density of air  $\rho$ , adiabatic sound speed  $c$  in air, angular frequency  $\omega$ , Prandtl number  $N_{\text{Pr}} = 0.71$ , and specific-heat ratio  $\kappa = 1.4$ .

### Exponential porosity model

The exponential porosity model [44] yields an expression only for  $Z$ :

$$Z = 0.484\left(\frac{\sigma}{f}\right)^{0.5} + i\left[0.484\left(\frac{\sigma}{f}\right)^{0.5} + 30\frac{\alpha}{f}\right]. \quad (\text{A5})$$

Material parameters are: flow resistivity  $\sigma$  and rate of porosity decrease with depth  $\alpha$ .

### Hybrid model

A hybrid model [7] is used for absorbing materials such as mineral wool. This model is equal to the Delany and Bazley model at high frequency ( $f > f_2$ ) and the Hamet model at low frequency ( $f < f_1$ ), with  $f_1 = 0.012\sigma/\rho$  and  $f_2 = 0.024\sigma/\rho$ . For  $f_1 \leq f \leq f_2$ , linear interpolation is used. If the impedance according to the model of Hamet *et al.* is denoted as  $Z_{\text{H}}$  and the impedance according to the model of Delany and Bazley as  $Z_{\text{DB}}$ , then the impedance according to the hybrid model is given by:

$$Z = \begin{cases} Z_{\text{H}} & \text{for } f < f_1, \\ \frac{f-f_1}{f_2-f_1} Z_{\text{DB}} + \frac{f_2-f}{f_2-f_1} Z_{\text{H}} & \text{for } f_1 \leq f \leq f_2, \\ Z_{\text{DB}} & \text{for } f > f_2. \end{cases} \quad (\text{A6})$$

For the complex wavenumber an analogous relation is used.

### Acknowledgement

This research work has been carried out within the context of the European *Harmonoise* project partially funded by the European Commission in the 5th framework IST Program (number IST-2000-28419). The authors are grateful to the French Department of Ecology and Sustainable Development (Ministère de l'Ecologie et du Développement Durable, Mission Bruit) and also to the UK DfT (Department of Transport) and DEFRA (Department of the Environment, Food and Rural Affairs) for financial support.

### References

- [1] J. E. Piercy, T. F. Embleton, L. Sutherland: Review of noise propagation in the atmosphere. *J. Acoust. Soc. Am.* **61** (1977) 1403–1418.
- [2] K. Attenborough et al.: Benchmark cases for outdoor sound propagation models. *J. Acoust. Soc. Am.* **97** (1995) 173–191.
- [3] T. F. Embleton: Tutorial on sound propagation outdoors. *J. Acoust. Soc. Am.* **100** (1996) 31–48.
- [4] T. Van Renterghem, E. M. Salomons, D. Botteldooren: Efficient FDTD-PE model for sound propagation in situations with complex obstacles and wind profiles. *Acta Acustica united with Acustica* **91** (2005) 671–679.
- [5] F. van der Eerden, E. Védý: Propagation of shock wave from source to receiver. *Noise Control Engineering Journal* **53** (2005) 87–93.
- [6] Harmonoise WP2 team: Definition of the physical problem. TNO Report HAR21TR-020129-TNO10, March 2002.

- [7] Harmonoise WP2 team: Task 2.2: State-of-the-art of modeling. TNO Report HAR22-TR020220-TNO10, October 2002.
- [8] Harmonoise WP2 team: Task 2.3: Benchmark calculations and modelling approximations. TNO Report HAR23-TR020222-TNO10, November 2002.
- [9] Harmonoise WP2 team: Task 2.4: Choice of basic sound propagation models. TNO Report HAR25TR-021018-TNO10, December 2002.
- [10] Harmonoise WP2 team: Task 2.5: Modeling solutions and algorithms. TNO Report HAR25TR-021104-TNO06, November 2003.
- [11] Harmonoise WP2 team: Task 2.6 and 2.7: Test calculations of day-evening-night levels. TNO Report HAR26TR-031113-TNO02, September 2004.
- [12] Harmonoise WP1.1 team: Source modelling of road vehicles. SP Report HAR11TR-020614-SP09v8, October 2004.
- [13] Harmonoise WP1.2 team: Railway source database, user manual. SNCF Report HAR12TR-040112SNCF02, January 2004.
- [14] Harmonoise WP2-WP3-WP4 teams: Task 2.8, deliverable 21: Validation of the harmonoise models. TNO Report HAR28TR-041109-TNO10.doc, December 2004.
- [15] D. van Maercke, J. Defrance: Development of an analytical model for outdoor sound propagation within the Harmonoise project. *Acta Acustica united with Acustica* **93** (2007) (same issue).
- [16] E. M. Salomons, J. D. van der Toorn: Calculation of traffic noise levels. HAR21-MO020204-TNO01, February 2002.
- [17] F. Aballéa, J. Defrance: Multiple reflection phenomena under meteorological conditions using the PE method with a complementary Kirchhoff approach. *Acta Acustica united with Acustica* **93** (2007) 22–30.
- [18] D. Heimann: Reference model, modeling solutions and algorithms: A unified meteorological classification. DLR Report HAR25MO-031121-DLR02, November 2003.
- [19] D. Heimann, E. M. Salomons: Testing meteorological classifications for the prediction of long-term average sound levels. *Applied Acoustics* **65** (2004) 925–950.
- [20] P. H. Parkin, W. E. Scholes: The horizontal propagation of sound from a jet engine close to the ground, at Hatfield. *Journal of Sound and Vibration* **2** (1965) 353–374.
- [21] V. E. Ostashev, E. M. Salomons, S. F. Clifford, R. J. Lataitis, D. K. Wilson, P. Blanc-Benon, D. Juvé: Sound propagation in a turbulent atmosphere near the ground: A parabolic equation approach. *J. Acoust. Soc. Am.* **109** (2001) 1894–1908.
- [22] R. Blumrich, D. Heimann: A linearized Eulerian sound propagation model for studies of complex meteorological effects. *J. Acoust. Soc. Am.* **112** (2002) 446–455.
- [23] ISO 9613-1: Acoustics – Attenuation of sound during propagation outdoors - Part 1: Calculation of the air absorption of sound by the atmosphere. 1993.
- [24] K. E. Gilbert, M. J. White: Application of the parabolic equation to sound propagation in a refracting atmosphere. *J. Acoust. Soc. Am.* **85** (1989) 630–637.
- [25] M. West, K. E. Gilbert, R. A. Sack: A tutorial on the parabolic equation (PE) model used for long range sound propagation in the atmosphere. *Applied Acoustics* **37** (1992) 31–49.
- [26] E. M. Salomons: Computational atmospheric acoustics. Kluwer, Dordrecht, 2001.
- [27] E. M. Salomons: Diffraction by a screen in downwind sound propagation: a parabolic-equation approach. *J. Acoust. Soc. Am.* **95** (1994) 3109–3117.
- [28] K. E. Gilbert, X. Di: A fast Green's function method for one-way sound propagation in the atmosphere. *J. Acoust. Soc. Am.* **94** (1993) 2343–2352.
- [29] E. M. Salomons: Improved Green's function parabolic equation method for atmospheric sound propagation. *J. Acoust. Soc. Am.* **104** (1998) 100–111.
- [30] N. Barrière, Y. Gabillet: Sound propagation over a barrier with realistic wind gradients. Comparison of wind tunnel experiments with GFPE computation. *Acta Acustica united with Acustica* **85** (1999) 325–334.
- [31] R. A. Sack, M. West: A parabolic equation for sound propagation in two dimensions over any smooth terrain profile: the generalised terrain parabolic equation (GT-PE). *Applied Acoustics* **45** (1995) 113–129.
- [32] E. M. Salomons: Sound propagation in complex outdoor situations with a non-refracting atmosphere: model based on analytical solutions for diffraction and reflection. *Acta Acustica united with Acustica* **83** (1997) 436–454.
- [33] R. D. Ciskowski, C. A. E. Brebbia: Boundary element methods in acoustics. Elsevier, London, 1991.
- [34] P. Jean: A variational approach for the study of outdoor sound propagation and application to railway noise. *Journal of Sound and Vibration* **212** (1998) 275–294.
- [35] P. Jean, J. Defrance, Y. Gabillet: The importance of source type on the assessment of noise barriers. *Journal of Sound and Vibrations* **226** (1999) 201–216.
- [36] T. van Renterghem, E. M. Salomons, D. Botteldooren: Efficient FDTD-PE model for sound propagation in situations with complex obstacles and wind profiles. *Acta Acustica united with Acustica* **91** (2005) 671–679.
- [37] D. Heimann, M. Bakermans, J. Defrance, D. Kühner: Vertical sound speed profiles determined from meteorological measurements near the ground. *Acta Acustica united with Acustica* **93** (2007) (same issue).
- [38] J. A. Businger, J. C. Wyngaard, Y. Izumi, E. F. Bradley: Flux-profile relationships in the atmospheric boundary layer. *J. Atmos. Sci.* **28** (1971) 181–189.
- [39] C. A. Paulson: The mathematical representation of wind speed and temperature profiles in the unstable atmospheric surface layer. *J. Appl. Meteor.* **9** (1970) 857–861.
- [40] E. M. Salomons, K. B. Rasmussen: Numerical computation of sound propagation over a noise screen based on an analytic approximation of the wind speed field. *Applied Acoustics* **60** (2000) 327–341.
- [41] J. Defrance, L. Bouilloud, E. Premat, P. Jean: 3D efficiency of some road barrier crownings using a 2D  $\frac{1}{2}$ -BEM. Proc. EuroNoise, Napoli, Italy, 19–21 May 2003 and *Acta Acustica united with Acustica* **89** (2003) Suppl.1, S70.
- [42] M. E. Delany, E. N. Bazley: Acoustic properties of fibrous absorbent materials. *Applied Acoustics* **3** (1970) 105–116.
- [43] M. C. Bérengier, M. R. Stinson, G. A. Daigle, J. F. Hamet: Porous road pavements: Acoustical characterization and propagation effects. *J. Acoust. Soc. Am.* **101** (1997) 155–162.
- [44] G. A. Daigle, M. R. Stinson, D. I. Havelock: Use of the PE method for predicting noise outdoor. Proc. Internoise 96, Liverpool, UK, 1996, 561–566.